

A novel micronemal protein MP38 is involved in the invasion of merozoites into erythrocytes

Tuyet-Kha Nguyen,¹ Sy-Thau Nguyen,^{1,2} Van-Truong Nguyen,¹ Sung-Hun Na,³ Robert W. Moon,⁴ Jetsumon Sattabongkot,⁵ Yee Ling Lau,⁶ Won-Sun Park,⁷ Wan-Joo Chun,⁸ Feng Lu,⁹ Seong-Kyun Lee,¹ Jin-Hee Han,¹ Eun-Taek Han¹

AUTHOR AFFILIATIONS See affiliation list on p. 16.

ABSTRACT The absence of an *in vitro* cultivation system for *Plasmodium vivax* hinders the exploration of molecular targets for vaccine development. To address this, functional studies often rely on alternative models, such as *P. knowlesi*, due to its genetic similarity to *P. vivax*. This study investigated the role of a novel micronemal protein, PvMP38 (PVX_110945), in both *P. vivax* and *P. knowlesi* merozoite invasion of erythrocytes. The full-length ectodomain of PvMP38 was expressed, and polyclonal antibodies were generated to assess its function. PvMP38 was confirmed to localize on micronemal organelle in both *P. vivax* and *P. knowlesi* merozoites. *In vitro* protein-protein interaction assays revealed that PvMP38 binds to Pv12 with high-affinity interaction. A conserved novel complex of Pv12-Pv41-PvMP38 was identified by immunoprecipitation of *P. vivax* antibodies on *P. knowlesi* schizont lysates. Linear epitopes of PvMP38 with high and moderate antigenicity were identified in clinical isolates of both species. Invasion inhibition assays demonstrated that a triple antibody combination targeting the PvMP38, Pv12, and Pv41 significantly reduced *P. knowlesi* merozoite invasion of erythrocytes compared to a single antibody. In addition, CRISPR/Cas9-mediated knockout of *P. knowlesi mp38* markedly impaired parasite growth, underscoring its essential role during the asexual stage. These findings identify PvMP38 and its associated complex as promising targets for malaria interventions and highlight the utility of *P. knowlesi* as a model for investigating *P. vivax* erythrocyte invasion mechanisms.

IMPORTANCE This manuscript reported an effort in malaria eradication by identifying and functionally characterizing a novel *Plasmodium vivax* micronemal protein, PvMP38, involved in erythrocyte invasion. A narrow repertoire of an efficacious vaccine targeting *P. vivax* candidates is being developed due to the lack of continuous *in vitro* culture. This study addresses a gap in *P. vivax* research using *P. knowlesi* as a model for both genome editing and antibody functionality validation. By enhancing the protein-protein interaction screening framework, this study demonstrated that PvMP38 forms a complex with Pv12 and Pv41, opening the approaches to multi-antigen vaccines. The successful application of CRISPR/Cas9 gene editing techniques to disrupt its homolog, the *pkmp38* gene, further assesses the protein's significance in the growth and invasion of the parasite. These findings provided valuable insights into the biology of *P. vivax* and proposed PvMP38 as a promising candidate for malaria intervention strategies.

KEYWORDS malaria, *Plasmodium vivax*, PvMP38, micronemal protein, complex formation, CRISPR/Cas9

Among the five *Plasmodium* species that infect humans, *P. vivax* is a significant cause of morbidity, particularly in Southeast Asia. Most *P. vivax*-related mortality occurs during the asexual blood stage, underscoring the need for developing vaccines targeting this stage (1). Current vaccine efforts have focused on mimicking natural immunity to

Invited Editor Niraj Harish Tolia, National Institute of Allergy and Infectious Diseases, Rockville, Maryland, USA

Editor L. David Sibley, Washington University in St. Louis School of Medicine, St. Louis, Missouri, USA

Address correspondence to Eun-Taek Han, ethan@kangwon.ac.kr.

The authors declare no conflict of interest.

See the funding table on p. 16.

Received 9 January 2025

Accepted 21 February 2025

Published 9 April 2025

Copyright © 2025 Nguyen et al. This is an open-access article distributed under the terms of the [Creative Commons Attribution 4.0 International license](https://creativecommons.org/licenses/by/4.0/).

inhibit parasite invasion and erythrocyte development (2, 3). Despite *P. vivax* Duffy-binding protein region II (PvDBPII) showing heterologous protection in Phase I/IIa clinical trials, vaccines targeting multiple *dbpII* alleles elicit higher responses than a single allele because of the high polymorphic properties (4, 5). Other studies also have indicated that single antigens induce protection against the homologous but not heterologous strains (6, 7). Therefore, a systematic approach to investigate additional candidates is needed to understand the *P. vivax* invasion mechanism and increase the chance of generating effective multivalent blood-stage vaccines.

The paucity of vaccine candidates characterized, particularly for *P. vivax*, is a consequence of several technical obstacles: (i) *P. vivax* only invades reticulocytes, limiting continuous *in vitro* cultivation (8), (ii) difficulties in expressing membrane-bound proteins in soluble form, and (iii) sensitivity limitations in detecting low-affinity protein-protein interaction (PPI) hinder the exploration of a new blood-stage candidate (9–11). These challenges necessitate the use of alternative models to study their invasion mechanisms. *P. knowlesi*, a zoonotic parasite with a close phylogenetic relationship and antigen cross-reactivity with *P. vivax* (12, 13). Unlike *P. vivax*, *P. knowlesi* can be cultivated in human erythrocytes *in vitro*, providing the opportunity to explore the invasion mechanisms (14). The advance of clustered regularly interspaced palindromic repeats (CRISPR)-Cas9 genomic modification in *P. knowlesi* has made it possible to validate *P. vivax* vaccine candidates by replacing *P. knowlesi* genes with their *P. vivax* counterparts (15). In addition, HEK293E mammalian cell expression was applied for correctly folded recombinant *P. vivax* proteins with post-translational modifications resembling native parasites (16, 17).

High-throughput analysis of *P. vivax* ectodomain libraries previously identified fundamental molecular interactions, including Pv12-Pv41 and novel Pv12-PVX_110945 (hypothetical protein) (8, 17), which were predicted to have essential roles in blood-stage parasites. Pv12 belongs to the 6-Cys gene family, which includes proteins released onto the surface of merozoites tethered by glycosylphosphatidylinositol (GPI)-anchor and forming interactions with merozoite membrane-bound proteins such as Pv41 (17, 18). Pv12 and Pv41 responded strongly to *P. vivax*-infected Korean patients' sera with 49% and 62.5% seropositivity, respectively (18, 19). Thus, the predicted complex formation involving Pv12 (rhoptry), Pv41 (surface), and a hypothetical protein, PVX_110945 (microneme in this study) is expected to be sequentially released during erythrocyte invasion and elicit a high immune response to vivax patients.

This study is the first to characterize PvMP38 (PVX_110945, estimated 38 kDa) as a novel micronemal protein involved in a complex formation with Pv41 and Pv12. It plays an essential role in understanding the parasite's invasion mechanism with its subcellular distribution. To further explore this, *P. knowlesi mp38*, a homolog of *Pvmp38*, was knocked out via CRISPR/Cas9 and systematically tested the invasion inhibition activity of different antibody cocktails, allowing us to precisely attribute effects to direct targeting of MP38.

RESULTS

Full-length ectodomain protein expression and polyclonal antibody production

As proof of concept for this study, which targets protein function and establishes PPI systems for *P. vivax*, the full-length extracellular domains of recombinant proteins were fused with His- or Fc-tags following the schematics shown in Fig. 1A. The phylogenetic relationship exhibited a pairwise identity of 55.5% with our research model, *P. knowlesi* (Fig. 1B) and had a high degree of conservation among its orthologs in other *Plasmodium* species (Fig. S1). The expressed recombinant His-tagged PvMP38 protein was evaluated for denatured by SDS-PAGE and native antigens by BN-PAGE (Fig. 1C). Recombinant PvMP38 protein was consistently detected as three bands, approximately 35, 43, and 63 kDa, under denaturing conditions. These three bands were confirmed using LC-MS analysis and matched the sequence of the identified protein ID, XP_001608414.1, with extensive homology (P -value < 0.05) (Table S1). The native gel analysis showed PvMP38

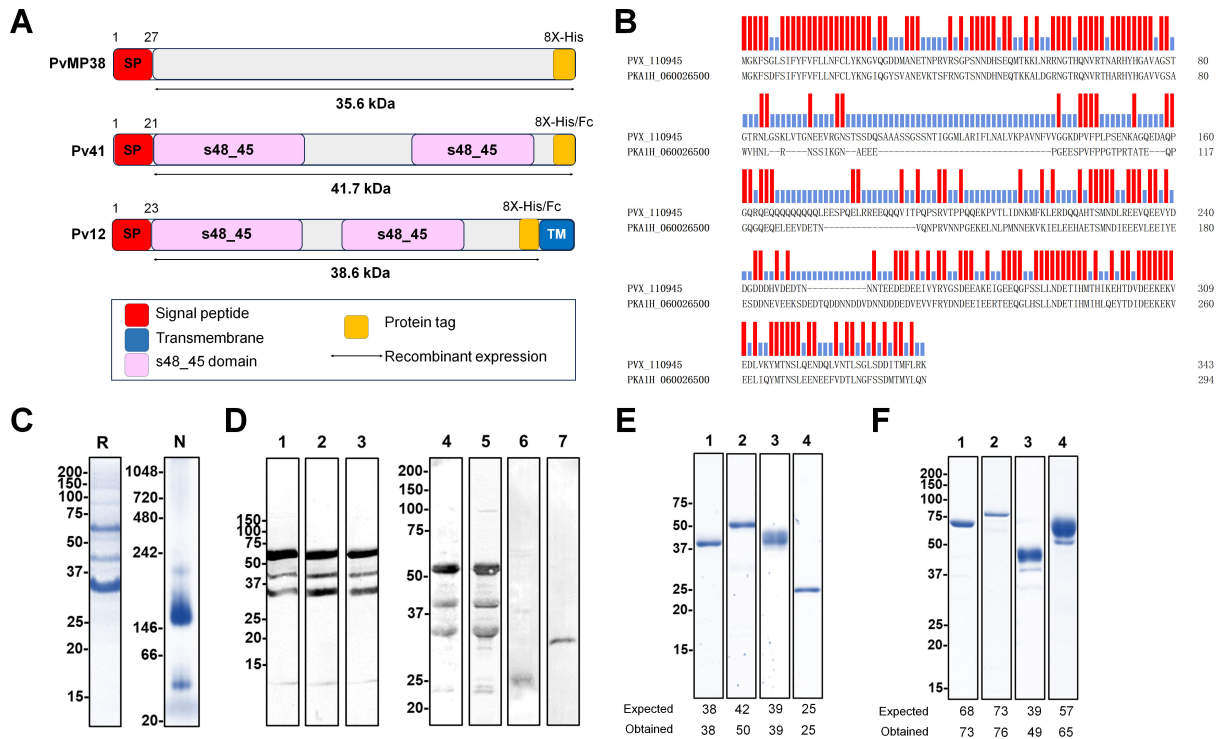


FIG 1 Recombinant protein expression. (A) Schematic structure of target proteins. (B) Amino acid sequence alignment of PVX_110945 (PvMP38) with orthologs in *P. knowlesi*, PkA1H_060026500 (PkMP38), the similarity is highlighted in red. The percent identity and divergence were analyzed using Clustal-W. (C) Recombinant PvMP38 (~37.8 kDa with 8x His tag) under reducing (R) and native condition (N). (D) Western blot analysis of recombinant PvMP38 probed with anti-His tag antibody for the positive control (lane 1), mouse- (lane 2), and rabbit-immune sera (lane 3). Recognition of the native PvMP38 antigen in the *P. knowlesi* schizont parasite lysate with mouse and rabbit antisera raised against the recombinant PvMP38 under reducing conditions (lanes 4 and 5) and the specificity confirmation by pre-immune mouse and rabbit sera (lanes 6 and 7). For protein-protein interaction analysis, other proteins were expressed with His-tag (E) and Fc-tag (F). Pv12 and Pv41 were expressed under His-tag (E, lanes 1 and 2) and were fused with Fc-tag (F, lanes 1 and 2). For positive and negative controls of protein-protein interaction analysis, PvDBP-RII-His (E, lane 3), human DARC-Fc (F, lane 3), and GST under His- or Fc-tags (E and F, lanes 4) were also expressed, respectively.

migrated at a larger-than-expected size of approximately 150 kDa, while the predicted monomer molecular weight was 38 kDa, indicating oligomerization. Animal immune sera against PvMP38 were immunoblotted using recombinant protein and *P. knowlesi* schizont-enriched lysates for the specificity of produced antisera (Fig. 1D).

The expressed His- or human IgG1-Fc-tagged ectodomains of Pv12 and Pv41 were analyzed under reducing conditions (Fig. 1E and F, lanes 1 and 2). Under native conditions, their His-tagged forms appeared as major band sizes over 66 kDa, suggesting homodimer formation (Fig. S2). This has previously been observed in *P. vivax* P12 and P41 (17). As a positive control for the sensitivity of PPI systems (biolayer interferometry [BLI] and enzyme-linked immunosorbent assay [ELISA]), PvDBP-II-His (194–521 aa) and human DARC-Fc (1–63 aa) were expressed (Fig. 1E and F, lanes 3). Two GST proteins tagged with His and Fc fragments, respectively, were used as a negative control for interaction specificity (Fig. 1E and F, lanes 4).

In vitro PPI identification of PvMP38-Pv12 and/or Pv41

To measure PPI, ELISA and BLI experiments were performed (Fig. 2; Fig. S3; Table S2). ELISA detected the specific interactions between *P. vivax* P12 to Pv41 in both orientations and Pv12-Fc with PvMP38-His tag, but not Pv41-PvMP38 (Fig. 2A and B). In biochemical analyses of PPI, BLI showed a strong binding between PvMP38 and Pv12-Fc with a K_D value of 2.46 ± 0.12 nM but no detectable interaction with Pv41-Fc (Fig. 2C and F). The binding affinities of Pv12-Fc for Pv41 were measured at a K_D value of 14.15 ± 2.76 nM

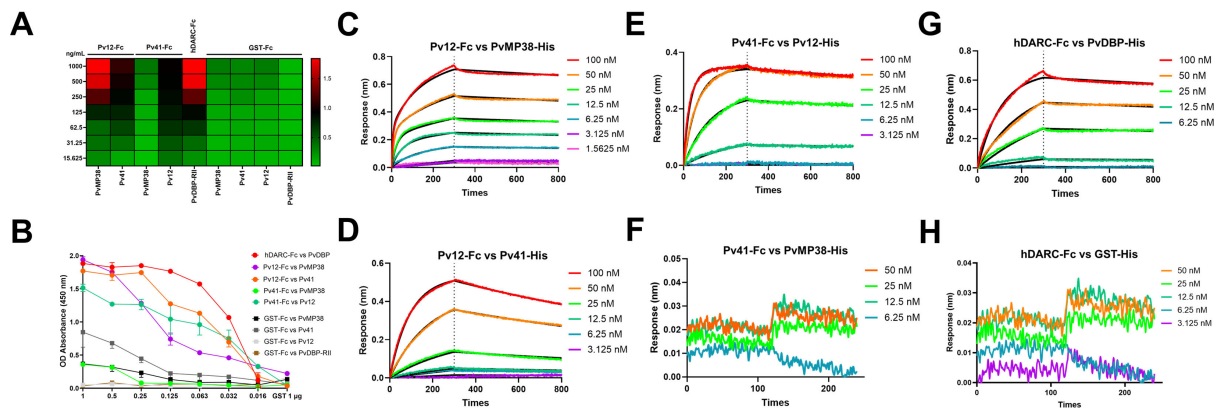


FIG 2 Identification and quantification of the protein-protein interactions. (A) Analysis of the interaction between Fc- and His-tagged recombinant protein by ELISA. (B) A line graph represents the ELISA absorbance of panel A; data points represent the means of two technical replicates, and error bars represent SD. (C–H) The recombinant His-tagged protein of each testing pair was injected over immobilized Fc-tagged recombinant protein. Raw data from two technical replicates of BLI experiments with different batches of protein in Table S2.

(Fig. 2D), while the reverse orientation resulted in a significantly higher affinity ($K_D = 0.53 \pm 0.03$ nM) (Fig. 2E). This BLI data indicated that although Pv12 interacted with both Pv41 and PvMP38, Pv41 did not bind PvMP38, with the equilibrium binding experiments between *P. vivax* P12 is showing a clear trend of dissociation saturation, suggesting the interaction’s specificity. The positive interaction between DARC-Fc and PvDBP-II-His was detectable at $K_D = 2.70 \pm 0.43$ nM without non-specific binding with GST-His protein (Fig. 2G and H). Interspecies binding compatibility was demonstrated as *P. knowlesi* P12 interacted with PvMP38 and Pv41 by recapitulating interactions using recombinant Pk12 (Fig. S3A through C). Although the native proteins had greater masses, no self-binding or non-specific interaction is observed with the negative control, GST protein (Fig. S3D).

Micronemal subcellular localization of PvMP38 in *P. vivax* and *P. knowlesi*-infected erythrocytes

Antibodies raised against the recombinant PvMP38 were used to explore the localization of MP38 within parasites. The anti-PvMP38 antibody specifically recognized *P. vivax* (Fig. 3A) and *P. knowlesi* parasites (Fig. 3B). These results showed that PvMP38 was co-localized with micronemal DBP (Fig. S4), displaying a distinct signal to rhoptry body RAMA, rhoptry neck RON2, and surface MSP1. The cross-reactivity between antibodies against recombinant *P. vivax* and *P. knowlesi* MP38 proteins was observed, indicating similar subcellular localization of both parasites. In addition, subcellular localizations of PvMP38 and Pv12 were analyzed from *P. vivax* and *P. knowlesi* WT (Fig. 3C) and E-64-treated parasites (Fig. 3D). Pv12 and PvMP38 were found to be located in adjacent apical loci, consistent with their respective localizations in rhoptry (Pv12) and microneme (PvMP38). This was seen in both segmented schizonts and egressed parasites. E64 treatment blocks egress but does not block the secretion of apical organelles; therefore, after incubation with this inhibitor, both MP38 and Pv12 were observed to be secreted onto the merozoite surface, where they then co-localized.

Impact of *pkmp38* deletion on blood-stage invasion efficiency and growth in *P. knowlesi*

To functionally characterize novel blood-stage antigens of *P. vivax*, we generated a CRISPR-Cas9-mediated knockout of *pkmp38*, the *pvmp38* ortholog, in *P. knowlesi*. The *pkmp38* gene was knocked out using a standard two-plasmid CRISPR-Cas9 system (Fig. 4A), and successful deletion was confirmed by genotyping with *pkmp38* locus-specific primers (Fig. 4B; Table S3). The WT *Pk* A1-H.1 parasite exhibited the expected band size containing the *pkmp38* gene, while the transfected parasite displayed the absence of

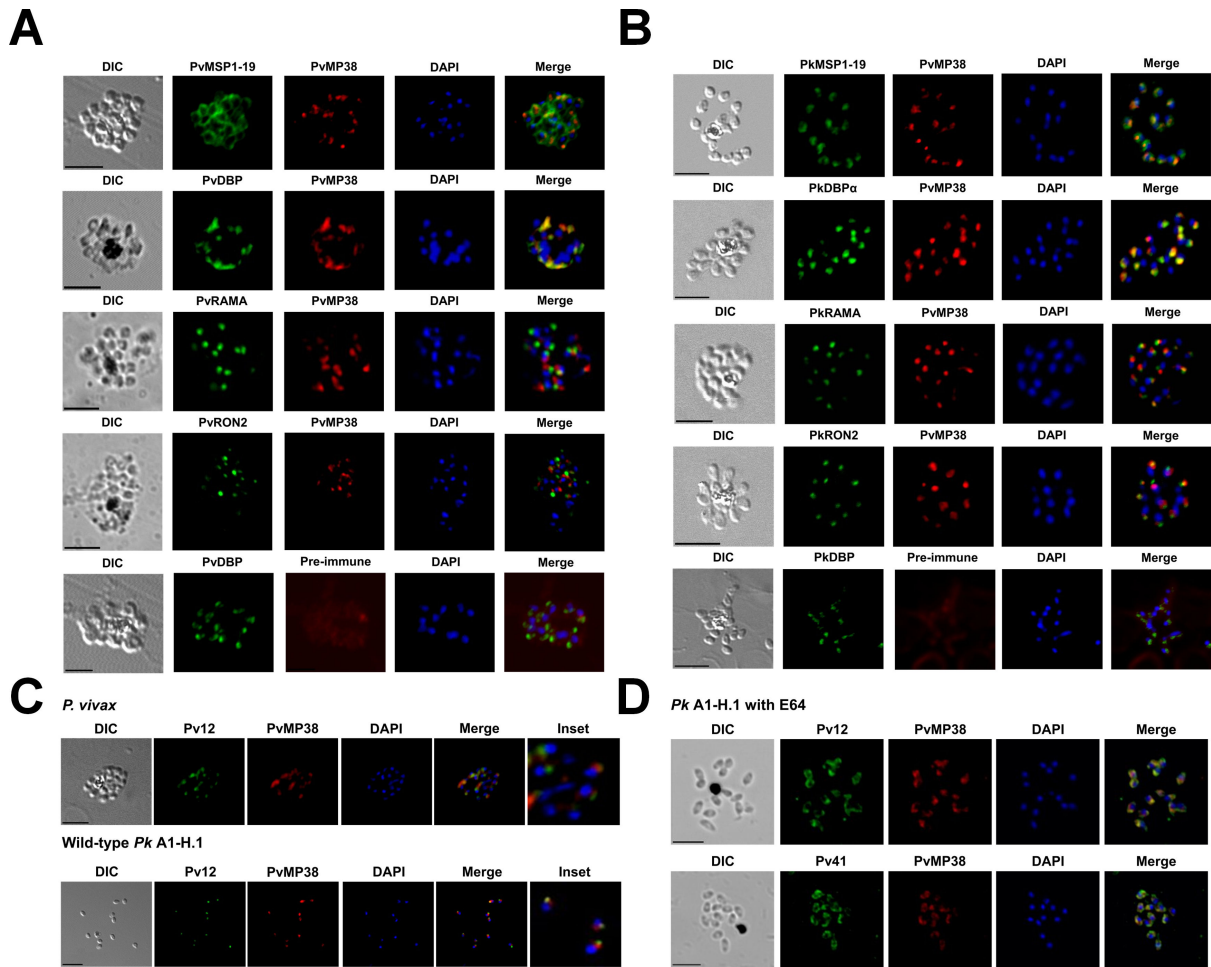


FIG 3 Subcellular localization of anti-PvMP38 with organelle-specific antibodies in the schizont stage of *P. vivax* (A)- and *P. knowlesi* (B)-infected parasites by immunofluorescence assay. (A) Reactivity of PvMP38 mouse polyclonal antibody (red) to *P. vivax* schizont-stage parasites co-localized with *P. vivax* surface protein, PvMSP1-19, microneme protein, PvDBP-II, rhoptry body (PvRAMA) and rhoptry neck protein (PvRON2) (each in green). (B) Cross-reactivity of mouse anti-PvMP38 (red) to *P. knowlesi* A1-H.1 schizont-stage parasites as red color co-localized with *P. knowlesi* surface protein, PkMSP1-19, microneme protein, PkDBPα-II, rhoptry body (PkRAMA) and rhoptry neck protein (PkRON2) (each in green). All samples were counterstained with antibodies raised from rabbits. (C) *P. vivax* and *P. knowlesi*, and (D) E64-treated *P. knowlesi* parasites were dual-labeled with rabbit antisera against Pv12/Pv41 (green) and mouse anti-PvMP38 (red). "Inset" panels depict enlarged regions. Non-specific staining is detected using PvMP38 pre-immune serum, proving the specificity of the produced antibody. Bars represent 5 mm. DAPI, 4',6'-diamidino-2-phenylindole.

this region, consistent with gene deletion verified by genome sequencing of WT and *Pkmp38*⁻ (KO) (Fig. S5A). The absence of PvMP38 ortholog expression in KO strain was demonstrated by the lack of specific signal in KO parasites in immunofluorescence assay (IFA) and immunoblotting using anti-PvMP38 antibody, whereas WT parasites displayed clear signals (Fig. 4C and D; Fig. S5B and C).

Growth inhibition assays revealed a significant reduction in the growth rate and replication efficiency of KO parasites compared to WT during the initial 10 replication cycles (Fig. 4E and F; Fig. S5D); however, KO parasites were allowed to recover growth rate after approximately 15 replication cycles (Fig. S5E). These findings establish that *pkmp38* plays a critical role in blood-stage parasite growth and invasion. In addition, the ability of KO parasites to adapt suggests that *P. knowlesi* can employ alternative pathways for erythrocyte invasion in the absence of PvMP38 ortholog expression.

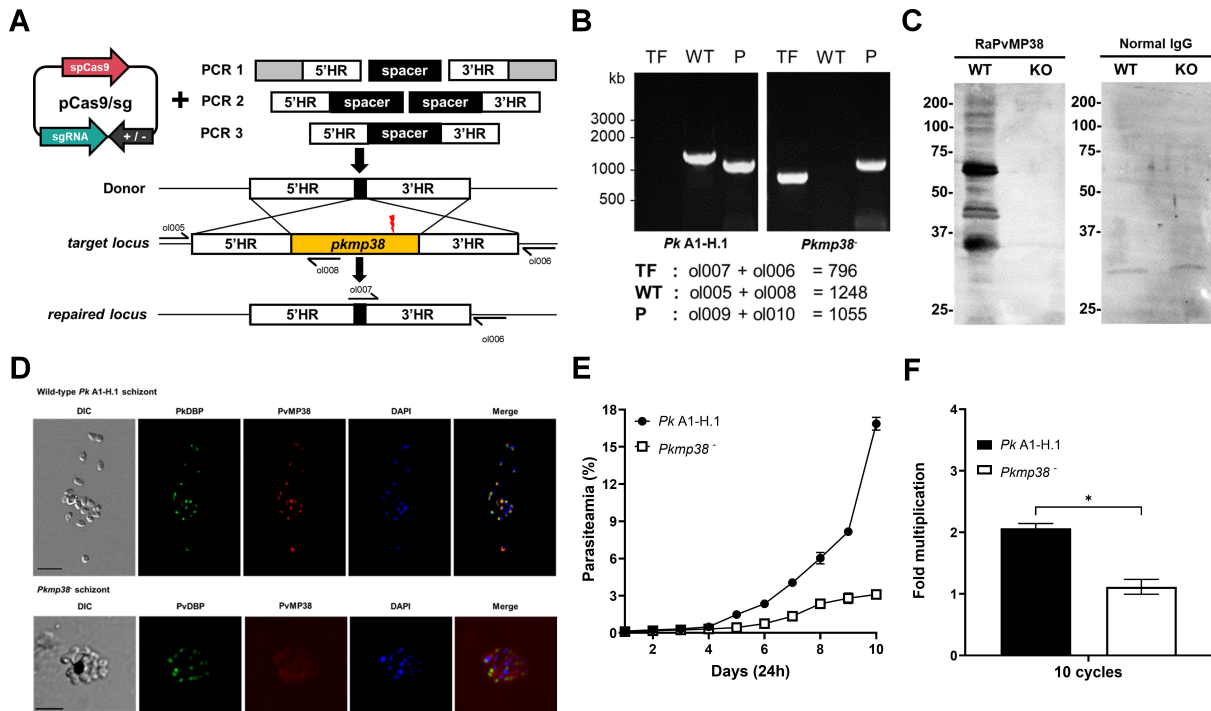


FIG 4 Disruption of *pkmp38*, an orthologue of *pvmp38*, in *P. knowlesi* parasites. (A) The donor DNA fragment was co-transfected with the pCas/sg construct that confers Cas9 nuclease, sgRNA, and drug resistance for further selection to knock out the *pkmp38* gene by double cross-over homologous recombination. The yellow box represents the barcode gene absent in the *P. knowlesi* genome for genotyping. Small black arrows indicate the primers. (B) Genotyping of parasite cloned out by limiting dilution. Target and disrupted fragments shown in panel A were amplified with primer pairs indicated in the box. TF, transfected parasites; WT, wild type; P, housekeeping gene. (C) Western blot analysis of WT and KO parasite lysates. Anti-PvMP38 recognized native antigens in *P. knowlesi* WT but not in KO parasite lysates. Non-immune rabbit IgG was used as a negative control. (D) Co-localization in *P. knowlesi* A1-H.1 (WT) and *Pkmp38* (KO) using polyclonal antibodies against PvMP38. Rabbit anti-PkDBP antibody (green) was dual labeled with mouse anti-PvMP38 antibody as a localization marker. (E and F) Parasitemia and multiplication rate at 10 cycles of *P. knowlesi* WT and KO were measured. After recovery from the knockout process, the initial parasitemia was diluted to less than 0.1% and followed up for 10 days. Significant differences in the effects of pre-immune sera and other antibodies were calculated using an unpaired *t*-test, *ns*, not significantly different $P > 0.05$; *, $P < 0.05$.

PPI among Pv12, Pv41, and PvMP38 from *P. knowlesi* WT and KO parasites

Co-immunoprecipitation assays were conducted to validate the interactions among Pv12, Pv41, and PvMP38 using WT and KO schizont-rich *P. knowlesi* parasite lysates (Fig. 5A). Initially, the presence of orthologs for Pv12, Pv41, and PvMP38 was confirmed in WT parasites (Fig. 5B). Western blot demonstrated that rabbit anti-Pv12 and -PvMP38 antibodies successfully co-immunoprecipitated both Pv41 + PvMP38 and Pv12 + Pv41 orthologs in WT parasites, respectively. While using rabbit anti-Pv41 antibody could pull down Pv12 and Pv41, but not PvMP38 (Fig. 5C). This could be attributed to the low affinity of anti-Pv41 antibody for the complex or steric hindrance, which might reduce the accessibility of the antibody when all three proteins are present. These limit the ability of the anti-Pv41 antibody to precipitate the entire complex, reflecting in the lower intensity band in the Pv12 signal (Fig. 5C, RaPv41). In KO parasites, only Pv12 and Pv41 bands could be detected using anti-Pv12 and -Pv41 antibodies, respectively. These results provide evidence for complex formation among Pv12, Pv41, and PvMP38 and highlight the conserved interspecies-specific epitopes that are presented within these antigens.

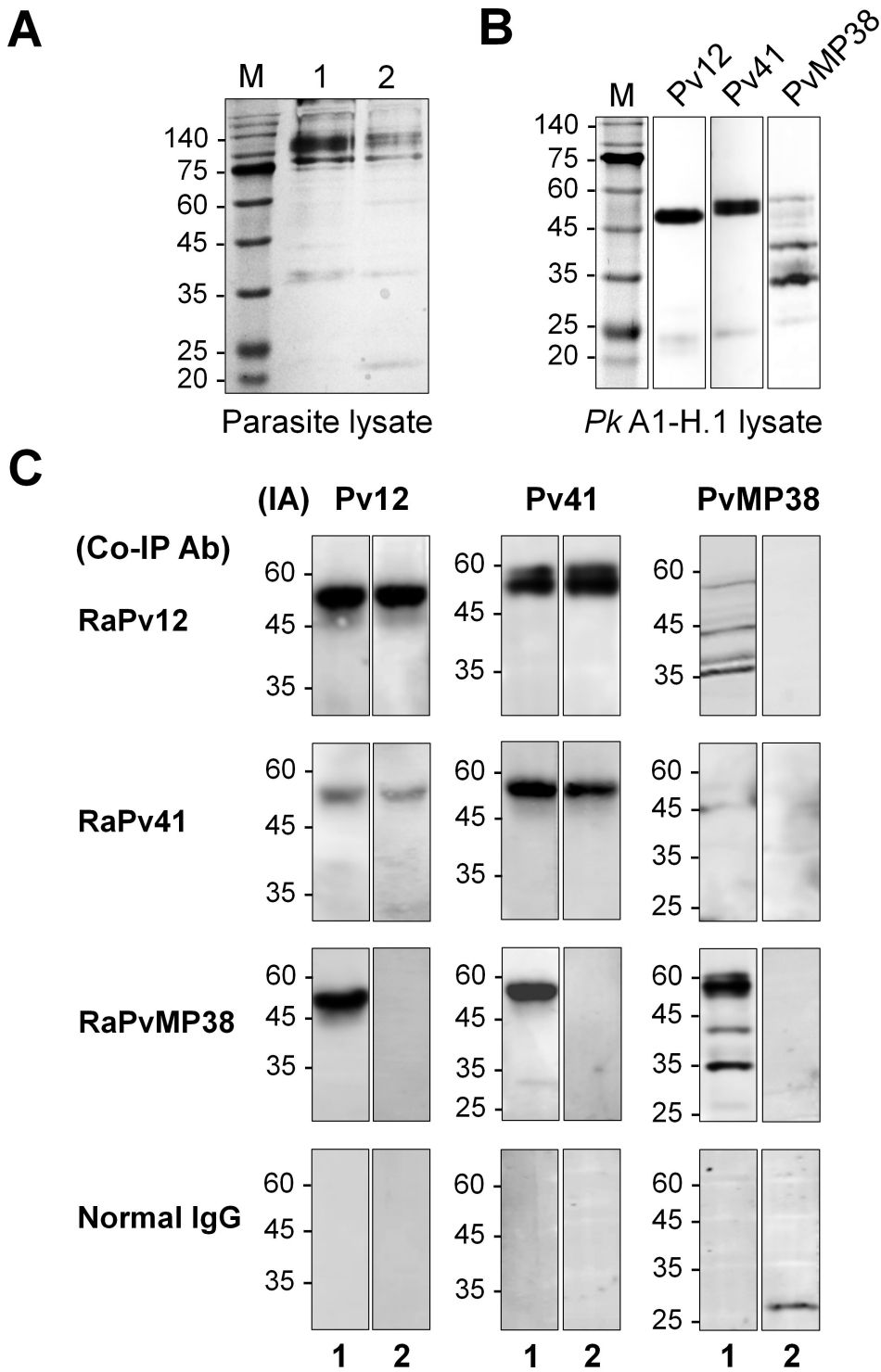


FIG 5 Co-immunoprecipitation assay using rabbit polyclonal antibodies (Co-IP Ab). (A) Total protein lysate from wild-type and knockout parasites were extracted and separated by 13% SDS-PAGE under reducing conditions, and followed by silver staining. (B) Specificity of mouse anti-Pv12, anti-Pv41, and anti-PvMP38 antibodies to recognize their orthologs in *P. knowlesi* by western blot analyses. (C) Western blot analyses were performed using mouse-raised antibodies to detect immunoprecipitated antigens (IA) in wild-type (lane 1) and knockout (lane 2) parasite, pulled down by rabbit sera against Pv12 (RaPv12), Pv41 (RaPv41), or PvMP38 (RaPvMP38). Normal rabbit IgG was used as a negative control for the co-immunoprecipitation assay.

Immunoreactivity and epitope specificity of PvMP38 in *P. vivax* and *P. knowlesi*-infected patients

To investigate the immune responses to PvMP38, a protein microarray was utilized to assess immunoreactivity against the full-length recombinant PvMP38 protein. Among *P. vivax* samples ($n = 72$), an IgG prevalence of 51.4% was observed (mean fluorescence intensity [MFI] = 1.076 ± 1.370 , 2 SD), while *P. knowlesi* samples ($n = 56$) exhibited an IgG response rate of 41.1% (MFI = $0.938 \pm .834$). Comparison between native and heat-treated antigens revealed that the immune response to PvMP38 predominantly targeted linearized epitopes. Denatured PvMP38 elicited a significant increase in immune responses from *P. vivax* patients, with seroreactivity rising from 51.4% to 70.8% (MFI = 2.001 ± 3.360), while a modest increase was observed for *P. knowlesi* samples, with sensitivity rising to 51.8% (MFI = $1.016 \pm .838$) (Fig. 6; Table S4). Thus, IgG responses to PvMP38 in *P. vivax* patient sera demonstrated high specificity compared to malaria-naïve sera, showing statistically significant differences. These findings highlight the immunogenicity of PvMP38 and its linear epitope specificity in *P. vivax* and *P. knowlesi* infections.

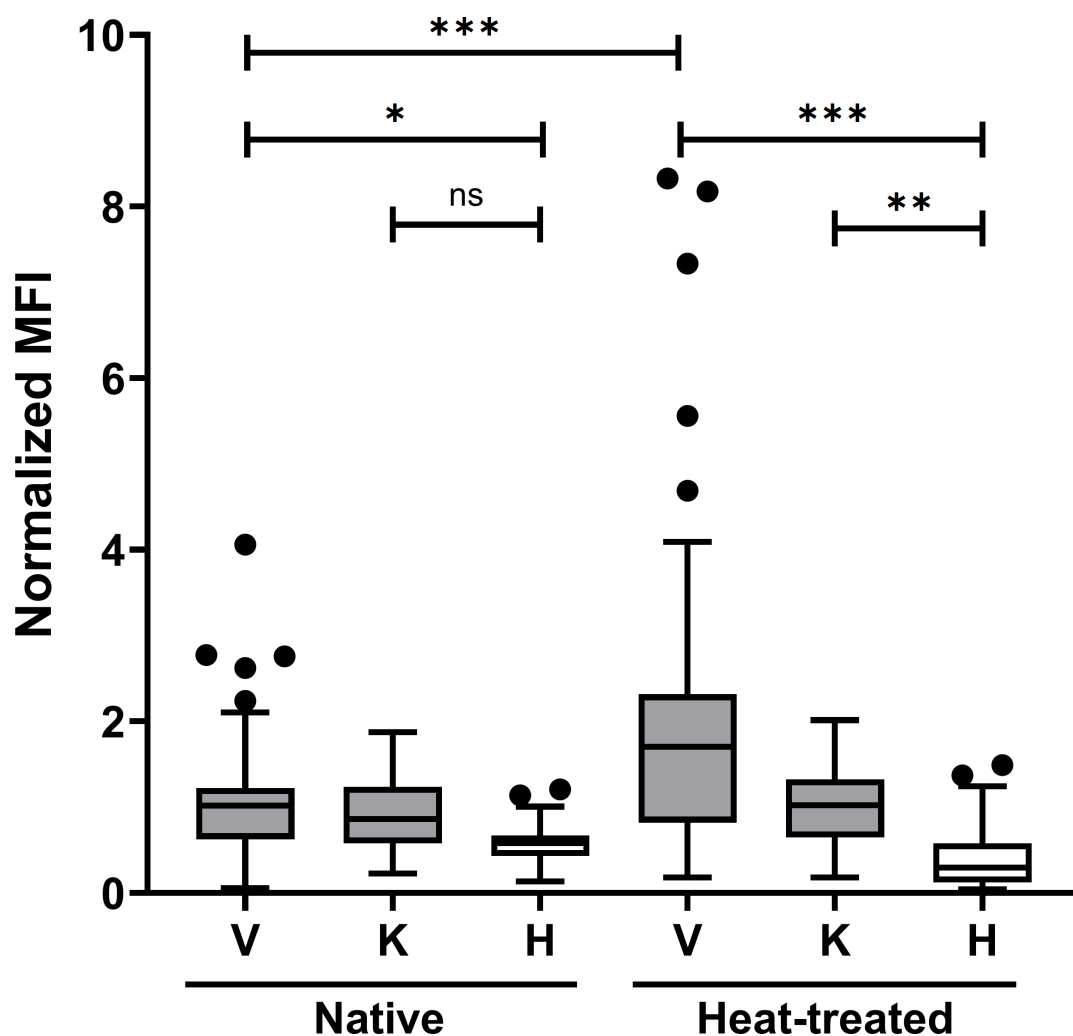


FIG 6 Humoral response of heat-treated and native PvMP38 to knowlesi (K) and vivax (V) patient sera. Normalized MFI represents the mean fluorescence intensity (MFI) divided by the cutoff value (equal to the mean fluorescence intensity plus two standard deviations (SDs) of the malaria-naïve samples). The bar indicates the mean \pm standard deviation. Individuals with outlier reactivity were indicated in the black dot. The prevalence of antibody response was compared to the patients and healthy individuals (H) using the multi-variant one-way ANOVA and Tukey's secondary test, ns, not significantly different $P > 0.05$; * $P < 0.05$; ** $P < 0.001$; *** $P < 0.0001$.

Additive inhibition of *P. knowlesi* merozoite invasion by antibodies targeting PvMP38, Pv12, and Pv41

This study identified PPIs involving the conserved epitope shared by *P. vivax* P12, P41, and MP38 orthologs in *P. knowlesi* parasite. To explore potential additive effects, we assessed combined antibody responses against WT and KO *P. knowlesi* parasites using purified polyclonal antibodies, tested individually and in combinations (double antibody and triple antibody) (Fig. 7). A single PvMP38 antibody exhibited dose-dependent inhibition of merozoite invasion, reaching $51.55\% \pm 1.25\%$ at 4 mg/mL in WT parasites. By contrast, the invasion inhibition in the KO parasite line was significantly reduced to $29.08\% \pm 2.15\%$, confirming that the PvMP38 antibody specifically targets its antigen (Fig. 7A). While the anti-Pv12 antibody alone showed less than 50% inhibition, its combination with other antibodies at 2 mg/mL significantly enhanced inhibition, with efficiencies ranging from $64.77\% \pm 0.05\%$ to $65.76\% \pm 0.90\%$ (Fig. 7B). Among the double antibody combination, the combination of anti-Pv41 and anti-PvMP38 antibodies (2 mg/mL each) inhibited invasion by $63.22\% \pm 2.01\%$, comparable to the anti-Pv12 plus anti-PvMP38 antibody combination. The most potent inhibition was observed with the triple-antibody combination (Pv12, Pv41, and PvMP38, at 1.3 mg/mL each), which resulted in $73.95\% \pm 1.91\%$ inhibition, outperforming individual antibodies at 4 mg/mL in WT parasites, indicating an additive inhibitory effect. In KO parasites, the antibody cocktail containing anti-PvMP38 antibodies reduced inhibition efficiency, while the Pv12 + Pv41 combination remained effective, suggesting that the other members of the complex remained critical targets in the absence of PvMP38. Furthermore, antibody combinations with anti-GST polyclonal antibodies exhibited no significant inhibition, confirming that the observed additive effect is specific to the Pv12-Pv41-PvMP38 complex.

DISCUSSION

Compared with *P. falciparum*, few *P. vivax* antigens have been described during the parasite invasion process due to the lack of a continuous *in vitro* culture system. Previous studies have investigated the molecular and cellular interaction of four important parasite ligands and erythrocyte (reticulocyte) receptors such as PvDBP-DARC (20), PvRBP2b-CD71 (21), PvRBP2a-CD98 (22), and PvEBP and CR1 (23)—making it clear that *P. vivax* invades host erythrocytes by establishing multiple distinct interactions with host receptors. Our previous reports identified important novel vivax molecules related to host cell invasion, including merozoite surface (19, 24), rhoptry (18, 25, 26), microneme (27, 28), dense granule, food vacuole (29), caveola-vesicle complexes (30), etc. However, many proteins, including PvMP38, remained poorly characterized.

In a previous study, a *hypothetical protein*, PvMP38, was briefly described; its transcription and genomic location suggested a function in merozoite development or erythrocyte invasion process; however, the extremely weak PPI with Pv12 neglected further study (17). In this study, we characterized PvMP38, a micronemal protein, by leveraging improved recombinant protein quality for PPI analysis and genetic modification in *P. knowlesi* parasites. To strengthen molecular interaction between these proteins, we employed a genetically engineered IgG Fc domain tag on the protein-binding partner, effectively enhancing the interaction avidity (31). This expression strategy increased interaction affinity (K_D value) between Pv12 and Pv41 sixfold compared to a previous report and enabled us to detect the Pv12/Pk12-PvMP38 interaction with high affinity. IgGs against PvMP38 were reacted on the microneme region in both *P. knowlesi* and *P. vivax* parasites, suggesting that the PPI complex may form among three main components of merozoite: PvMP38 (microneme in this study), Pv12 (rhoptry) (18), and Pv41 (surface) (19). Our co-immunoprecipitation assay further supported this hypothesis by demonstrating the mutual pull-down of these antigens, providing evidence for their interaction within the parasite, and IFA offered additional proof of the complex localization. Previous IFA studies of Pv12 in *P. vivax* (18) exhibited that it localizes to the rhoptry

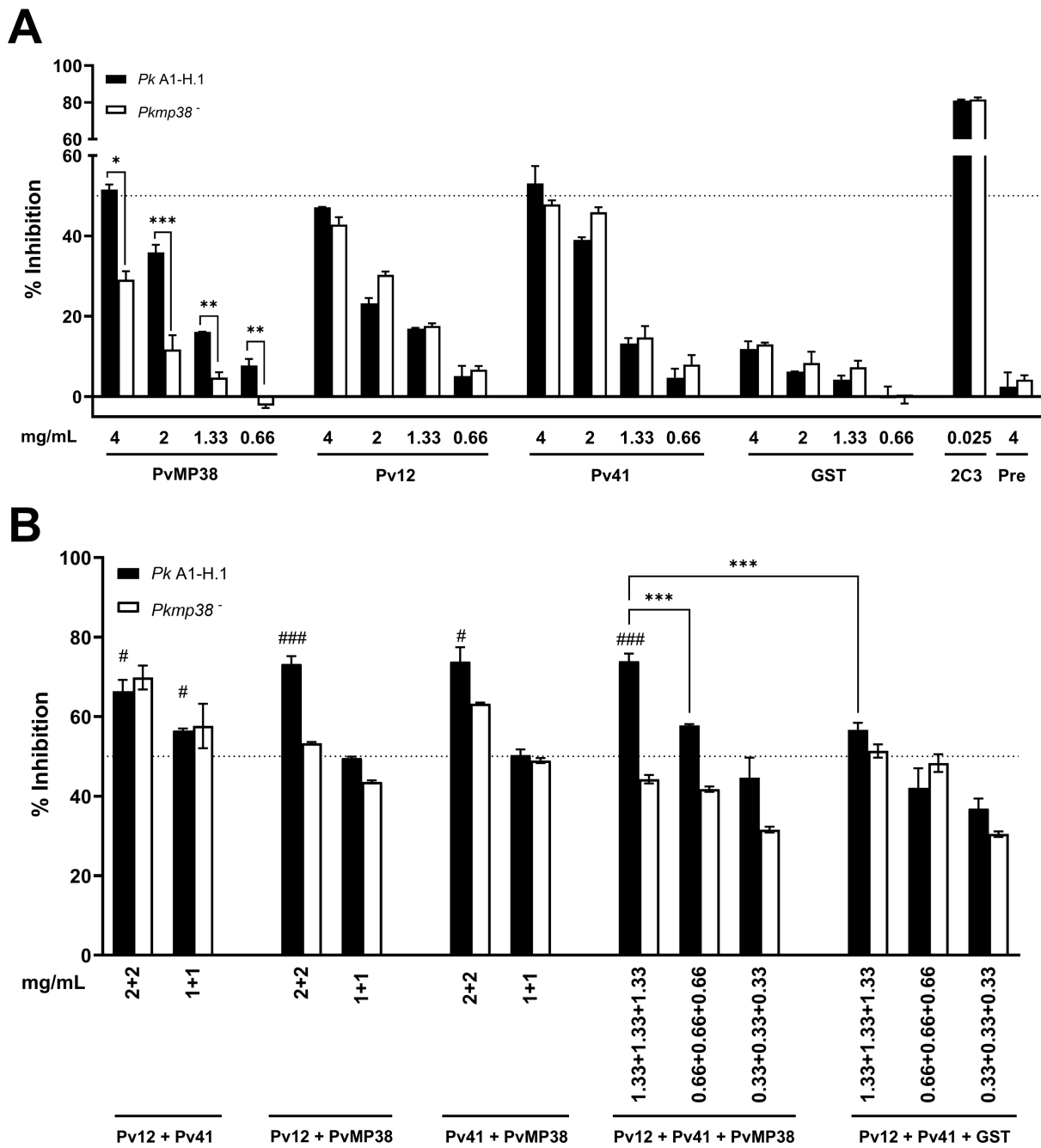


FIG 7 The invasion-inhibitory activity of *P. vivax* antibodies in single (A) and combination (B) against *P. knowlesi* A1-H.1. (A) Total IgGs purified from rabbit sera were tested individually for invasion-inhibitory activities (0.66 to 4.0 mg/mL). (B) Combinations of two IgGs were assessed at two concentrations (2.0 and 2.0 mg/mL, and 1.0 and 1.0 mg/mL), and combinations of three IgGs were tested at 0.33, 0.66, and 1.33 mg/mL each. 2C3 IgG (25 µg/mL) was used as a positive control. To determine whether the inhibition was statistically significant, all treatments were independently compared to the same concentration of total IgG of the negative control, which is the inhibition of purified IgG from pre-immune rabbit sera (single) combined with GST-his rabbit immunized (combination). Two independent assays were performed in duplicate. Significant differences in the effects of pre-immune sera and other antibodies were calculated using a multi-variant one-way ANOVA and Tukey's secondary test, [#]*P* < 0.05; ^{###}*P* < 0.01; ^{***###}*P* < 0.001. * represents the difference among groups within the graph. # represents the difference between single and combination antibody strategies, where 2 + 2 and 1 + 1 double combination sets (2 mg/mL and 1 mg/mL of each antibody) were compared with 4 mg/mL and 2 mg/mL of its single antibody components. A triple combination set of 1.33 + 1.33 + 1.33, 0.6 mg/mL, and 0.3 mg/mL each were compared with three single antibodies at 4, 2, and 1 mg/mL.

rather than the merozoite surface. Conversely, an experiment with *P. knowlesi* showed it resides in the merozoite surface (13). Given protein secretion during the invasion, the

E64-treated parasite was used to observe the translocation of target antigens to the merozoite surface. Interestingly, both Pv12 and PvMP38 were secreted from the apical organelle onto the E64-treated parasite surface and overlapped with the Pv41 signal, supporting co-localization and the potential for these proteins to form a complex during invasion (Fig. 3C and D). However, attempts to confirm these PPIs through re-orientation using Fc-tagged PvMP38 were unsuccessful due to precipitation caused by the increased protein size. There is currently no evidence for the structural configuration of this protein complex. Thus, experiments aimed at tracking the co-localization of these interactions within the parasites and/or structural analysis by cryo-EM may provide valuable insights into the biological evidence of these interacting pairs.

LC-MS analysis suggested the presence of truncated forms or structural isoforms of PvMP38, as the protein displayed multiple molecular weights under reducing conditions and formed oligomers on native PAGE. These differences could result from disulfide bond patterns or variations of hydrodynamic structure, indicating either a natively folded conformation or an elongated structure. Further investigation was conducted to define whether PvMP38 contains conformational or linear epitopes through heat treatment and assessed its serological activity in *P. vivax* and *P. knowlesi*-infected patients. Heat treatment denatured and disrupted the PvMP38 structure, exposing hidden linear epitopes, which led to a 20% increase in IgG reactivity in the vivax-positive patient serum samples, indicating that PvMP38 targets linear epitopes. Such structural insights would aid in distinguishing protective versus conformational epitopes, which could significantly impact vaccine candidate identification. Further research on these targets will benefit from target-specific methods, such as monoclonal antibodies or peptide mapping. Larger sample size screenings and assessment of antigen-specific IgG response durations following the *P. vivax* exposure would be needed to determine the scope of the IgG response in providing clinical defense.

For the first time, it was confirmed that the PvMP38 forms conserved PPIs or protein complexes with Pv12 and Pv41 across species, evidenced by cross-reactive interactions with *P. knowlesi* orthologs. We cannot rule out that PvMP38/Pk12 and Pk12/Pv41 form mutually exclusive complexes; however, this interaction is also crucial for functional activity and likely predates the evolutionary divergence of *P. knowlesi* and *P. vivax*. The co-immunoprecipitation revealed the complex formation among Pv12, Pv41, and PvMP38 in *P. knowlesi* using antibodies against *P. vivax* antigen, implying the existence of conserved interspecies epitopes within these antigens. The high conservation led us to use *P. knowlesi*, a human erythrocyte-adapted alternative model for *P. vivax*. Previous reports have emphasized the suitability of *P. knowlesi* as a model for *P. vivax* vaccine development (12, 13, 15, 31–34). This study successfully utilized the strengths of *P. knowlesi* to assess antibody efficacy and genetic tractability without a robust *P. vivax in vitro* cultivation system. However, some *P. vivax* proteins have orthologs in *P. knowlesi* that exhibit strong cross-reactivity; others do not, and certain *P. knowlesi* genes are not amenable to knockout, complicating research efforts (13). Therefore, employing various models, including the use of ortholog replacement approaches on *P. knowlesi*, *P. cynomolgi*, and *P. vivax ex vivo*, as well as transgenic rodent models, could provide a more precise approach to characterizing *P. vivax* antigens.

Gene KO experiments in *P. falciparum* P12 and *P. knowlesi* P41 have shown that these genes are not essential for invasion (13, 35). However, the inability to delete *pk12* in *P. knowlesi* in the previous study suggests that the *pk12* gene is essential for invasion and development (13). Thus, the functional role of Pv12 alternatively could mainly be evaluated through invasion inhibition assay (IIA) by target-specific IgG. In this study, *pkmp38* gene deletion hampered invasion and growth initially, but it was compensated by alternative invasion molecules in *P. knowlesi*. The slow recovery after the target gene KO process allows parasites to compensate for the loss of a specific gene. By contrast, IIAs validated in a single cycle may limit parasites from finding alternative ways to adapt. Understanding precisely how parasites are able to adapt to this pathway loss may also enable us to find synergistic combinations to block adaptation. Given that vaccines

targeting a single candidate (e.g., PvDBP and PvMSP1-19) (36, 37) are vulnerable to immune system evasion, a systematic approach using a combination of antibodies was applied to enhance protection against malaria. The additive inhibition effect of triple antibodies against PvMP38, Pv12, and Pv41 suggests a function in targeting distinct epitopes.

This study highlights the discovery of the novel micronemal protein PvMP38 and its conserved interactions with Pv12 and Pv41, alongside advancements in Fc-fusion protein expression and enhancing binding avidity in PPIs. Notably, the identification of PvMP38 represents a significant breakthrough, providing deeper insights into the mechanisms of *P. vivax* reticulocyte invasion. PvMP38 offers a new avenue for vaccine development, supporting a multi-antigen approach to improving immune responses and protection against malaria.

MATERIALS AND METHODS

Collection of malaria-infected patients' serum samples

P. vivax patient samples from the Republic of Korea from 2009 to 2011 and *P. knowlesi* patient samples from *P. knowlesi* endemic areas at the University of Malaya Medical Center (UMMC), Malaysia, between 2010 and 2013 were collected for humoral immune response analysis by protein array. A positive *P. vivax* sample from Thailand was used to purify parasites in the IFA. Healthy sera were from 10-year-old children with no malaria infection history from non-endemic regions in Gangwon Province Hospitals as a negative control. Information on parasite count, age, and sex obtained in this study is provided in Table S5.

Design and gene synthesis for plasmid DNA construction

All gene sequence data and protein information were obtained from the Plasmodium Genomics Resource (PlasmoDB: <http://plasmodb.org/plasmo/>) and GenBank websites (Table S6). The expected molecular weights of the *P. vivax* proteins and orthologous proteins in *P. knowlesi* were predicted using SnapGene software (GSL Biotech LLC, San Diego, CA). The amino acid sequence data were aligned using the CLUSTAL-W program in MegAlign Lasergene software (version 7.0, DNASTAR, Madison, WI). Sequences encoding the codon-optimized full-length ectodomain were obtained from the Addgene library (Addgene Inc., Watertown, MA). The optimized sequences were cloned into the pTT5-based expression vector. For the His-tagged expression, the endogenous signal peptide (leader sequence of human variable light chain) in the upstream region combined with 8×His C-terminal tag. The Fc-fusion vector was generated by fusing the human immunoglobulin Fc domain (HIgGk-Fc) tag.

HEK293 EBNA1-6E cell cultivation and recombinant protein purification

The HEK293-EBNA1 human cell line was adapted for suspension culture in FreeStyle F17 Medium (Life Technologies, Burlington, ON) at 37°C, 75% humidity, and 8% CO₂ with shaking at 125 rpm. Expression plasmids were transiently transfected using PEI (Polysciences, Inc., Warrington, PA) (38, 39). For His-tagged protein purification, the culture supernatant was incubated with Ni-NTA resin (QIAGEN, Hilden, Germany) at 4°C overnight. The mixture was loaded onto a Poly-Prep Chromatography column (Bio-Rad Inc., Hercules, CA) and washed with 10 mM imidazole, 300 mM NaCl, and 50 mM sodium phosphate (pH 7.4), followed by elution with 250 mM imidazole. For Fc-tagged proteins, the supernatant was passed through a 1 mL HiTrap Protein G HP column (GE Healthcare, Uppsala, Sweden) and purified according to the manufacturer's instructions. Eluates were buffer-exchanged into PBS using a 10 kDa Amicon Ultra-15 Centrifugal Filter (Merck Millipore, Darmstadt, Germany).

Production of animal immune sera and antibody purification

Six-week-old female BALB/c mice and Japanese white rabbits were used to generate polyclonal antibodies. Mice were injected with 30 μg , and rabbits 250 μg of His-tagged recombinant protein intraperitoneally with Freund's complete adjuvant (Sigma-Aldrich, St. Louis, MO), followed by Freund's incomplete adjuvant (Sigma-Aldrich) at 3-week intervals. Immune rabbit IgGs were purified using a protein G HP column following the manufacturer's protocol (GE Healthcare). The eluted IgG fractions were dialyzed into RPMI-1640 (Invitrogen/Gibco, Grand Island, NY) or PBS using a 10 kDa cutoff filter (Merck Millipore). Purified IgGs were pre-adsorbed with human O⁺ erythrocytes (25 μL of RBCs per 4 mg of IgGs) to remove non-specific inhibitory effects (32).

Gel electrophoresis and western blotting analyses

For quality assessment of the purified proteins and parasite lysates, blue native (BN)/13% SDS-PAGE/silver stain and western blot analyses were performed (40, 41). Samples were boiled with reducing buffer for SDS-PAGE or prepared with sample buffer for 4%–16% native-PAGE (Thermo Fisher Scientific, Cleveland, OH) and stained with Coomassie brilliant blue (Sigma-Aldrich) or Pierce Silver Stain Kit (Thermo Fisher Scientific). Western blot was analyzed by incubating with primary antibodies: mouse anti-6 \times His tag (1:2,000, ab18184, Abcam, Cambridge, MA), mouse anti-PvMP38 (1:500), and rabbit anti-PvMP38 (1:1,000). The membranes were then detected by secondary antibodies including IR Dye 680RD goat anti-mouse IgG, IR Dye 800CW goat anti-rabbit IgG, (LI-COR Inc., Lincoln, NE) and analyzed using the Odyssey infrared imaging system (LI-COR Inc.). For protein identification, bands were digested with trypsin, and peptides were analyzed by LC-MS/MS. Data were processed in Proteome Discoverer (v1.4) using Mascot v2.4 (Matrix Science, London, UK) with a cutoff ion score of 30 and a significance threshold of 0.05.

Biolayer interferometry analysis

BLI was used to measure protein-protein binding affinity and kinetics using the real-time Gator Label-Free Bioanalysis System (Gator Bio, Palo Alto, CA) with anti-human IgG Fc (HFC) probes. The biophysical binding affinity of the predicted interactions was analyzed with the one-to-one fit model. The probes were activated, followed by baseline (PBS, 90 s), Fc-tagged protein immobilization (10 μM , 120 s), washing (PBS, 90 s), serial dilution of His-tagged protein (1.5 to 100 μM , 300 s), and dissociation (PBS, 600 s). Binding affinities (K_D values) were calculated using a 1:1 global fitting model, with glutathione S-transferase (GST)-His as a negative control to assess nonspecific binding.

Enzyme-linked immunosorbent assay

For PPI analysis, Fc-tagged proteins (1 $\mu\text{g}/\text{mL}$) in a 0.1 M sodium carbonate buffer (pH 9.6) were coated to 96-well plates and incubated overnight. The interaction was assessed using serial dilutions of the partner proteins, and the interaction of hDARC-PvDBP and GST protein was used as positive and negative controls, respectively. The reaction detection was performed with HRP-conjugated anti-His tag antibodies (1:5,000), added substrate, and stopping the reaction; absorbance was measured at OD₄₅₀ by a PHERAstar plus instrument (BMG Labtech, Germany).

Serological analysis by protein microarray

As described previously, a protein microarray was performed to evaluate the antigenicity of PvMP38 in malaria patients and healthy individuals (42). Recombinant PvMP38 protein was applied onto the aminopropyl-coated slides at 100 ng/ μL . The amine chips were probed with serum samples from *P. vivax*-infected patients (Republic of Korea, $n = 72$), *P. knowlesi*-infected patients (Malaysia, $n = 56$), and 70 healthy individuals, diluted 1:25 in PBS-T in duplicate. Finally, 10 ng/ μL of Alexa Fluor 546-conjugated goat anti-human IgG (Invitrogen) in PBS-T was applied for data visualization. Fluorescent signals were scanned

using InnoScan 300 (INNOPSYS, France). To identify the epitope of an antigen, recombinant PvMP38 was heat-treated at 100°C for 5 minutes and proceeded as described above.

***In vitro* cultivation of *P. knowlesi*, synchronization, and native antigen extraction**

The *P. knowlesi* human-adapted strain (PkA1H1_HB) strain was cultured in 2% hematocrit following the previous protocol (43) with human O-type erythrocytes in a complete RPMI-1640 medium with supplements and gentamicin (Invitrogen) (44). Mature schizont-stage parasites were enriched using a gradient (40%/70%) Cytiva Percoll solution (Thermo Fisher) (26). The schizont-rich parasite was lysed by saponin, as previously described (45). The extracted mixtures were fractionated by SDS-PAGE and blotted onto the PVDF membrane, which was probed with PvMP38 rabbit IgG at 1 µg/mL as the primary antibodies.

CRISPR-Cas9 genome editing, transfection, and genotyping of *P. knowlesi* parasites

The templates were synthesized following the previous report (46). Briefly, the 5' and 3' homology regions (800 bp each) flanking the *pkmp38* guide were amplified with a 25-nucleotide overhang at the 3' and 5' ends from *P. knowlesi* genomic DNA. The final templates were pooled, ethanol-precipitated, and used as the 5' HR-*pkmp38*-3' HR construct for transfection. Three single-guide RNAs (sgRNAs) were screened using CRISPR REGEN Tools (47) and selected with high out-of-frame scores and a single on-target effect (Table S7). The pCas9/sg (15) vector was produced by cloning the annealing sgRNAs into BtgZI digested Cas9 vector. Primer sequences, primer combinations, and running conditions are listed in Tables S3, S8, and S9.

The tightly synchronized *P. knowlesi* parasites schizont was transfected using the Amaxa 4D electroporator (Lonza, Basel, Switzerland) and the P3 Primary cell 4D Nucleofector X kit L (Lonza), as previously described (44). Briefly, 20 µg of synthesized template (PCR products) and 20 µg pCas9/sg were mixed with P3 Primary cell nucleofector solution, including supplement 1 (Lonza). The DNA with 10 µL packed parasites mixture was transferred to a Nucleocuvette Vessel (Lonza), followed by a nucleofection program, FP158. Transfected parasites were selected by drug treatment with 100 nM pyrimethamine (Sigma-Aldrich). The transfected parasites were cloned out by limiting dilution and culture until the parasite appeared.

Indirect IFA analysis

The IFA was performed as described previously (12). Primary antibodies included mouse anti-PvMP38 (1:50) mixed with rabbit polyclonal antibodies specific to cellular locations of *P. knowlesi* and *P. vivax*: rabbit anti-RAMA (rhoptry body-specific antibody, 1:100), anti-RON2 (rhoptry neck-specific antibody, 1:100), anti-DBP (microneme-specific antibody, 1:250), and anti-MSP1-19 kDa (merozoite surface-specific antibody, 1:100). Secondary antibodies of Alexa 568-conjugated goat anti-mouse IgG and Alexa 488-conjugated goat anti-rabbit IgG (Invitrogen) were used at 1:500 dilution. Nuclei were stained with DAPI (4',6'-diamidino-2-phenylindole, Invitrogen). *P. knowlesi* A1-H.1 schizonts were treated with 10 µM of cysteine proteinase inhibitor (E64) (Sigma-Aldrich) for 2 hours to prevent egress and tested protein secretion with anti-Pv12 antibody (1:100). Slides were visualized using a motorized inverted fluorescence confocal microscope *ECLIPSE Ti2* (Nikon, Tokyo, Japan). Each fluorescence graphic was calculated using Image J (NIH, Bethesda, MD).

Invasion inhibition assay

P. knowlesi wild-type (PkA1-H.1, WT) and knockout (*Pkmp38*⁻, KO) strain schizonts, enriched by magnetic separation (MACS, Miltenyi Biotec, Rhine-Westphalia, Germany)

were adjusted to 1%–2% parasitemia (48). Well without and with an anti-Fy6 monoclonal antibody against the Duffy antigen/receptor for chemokines (DARC; clone 2C3; 25 µg/mL; Absolute antibody, Wilton, UK) were defined as normal invasion and antibody-mediated invasion inhibition. After one cycle of parasite growth (approximately 10 hours), the pellets were fixed with 0.05% glutaraldehyde (Sigma-Aldrich) and then stained with 0.2× SYBR Green I (Sigma-Aldrich). Two hundred thousand events were analyzed using an Accuri C6 flow cytometer (BD Biosciences, San Jose, CA). Inhibition of invasion of tested wells was compared to purified pre-immune IgG and rabbit IgG against GST-His proteins with the same adjuvant. Two independent experiments were performed in duplicate.

Co-immunoprecipitation

Co-immunoprecipitation was carried out using a Dynabeads Protein G Immunoprecipitation Kit (Thermo Fisher Scientific). Briefly, the Dynabeads-antibody complex was prepared by incubating rabbit polyclonal antibodies against Pv12, Pv41, and PvMP38 (diluted 1/100) with Dynabead Protein G for 30 minutes, rotation at RT; and normal polyclonal antibody was used for negative control. Then, the Dynabeads-Ab-antigen complex was prepared by adding the freshly extracted mature schizont of WT and KO parasites for 2 hours of rotation at RT. After washing twice with a washing buffer, proteins were eluted with an elution buffer and neutralized with 1 M Tris, pH 9.0. The supernatants were analyzed by western blot using mouse antibodies against Pv41, PvMP38, and Pv12 antibodies (diluted 1:500) as primary antibodies.

Data analysis

Data are presented as mean plus standard deviation (SD) for duplicate technical and biological replicate measurements. The data were analyzed using GraphPad Prism software version 10.1.2 (GraphPad, San Diego, CA). Student's *t*-test, a multi-variant one-way ANOVA, and Tukey's secondary tests were used to compare experimentally measured statistical differences (*P*-values) among groups. All kinetic assay data were observed using Gator® GatorOne v2.10 software (Gator Bio).

ACKNOWLEDGMENTS

PVX_110945-bio was a gift from Julian Rayner & Gavin Wright (Addgene plasmid # 68538; <https://www.addgene.org/68538/>; RRID: Addgene_68538).

This study was supported by a National Research Foundation of Korea (NRF) grant funded by the Korean government (MSIP) (NRF-2017R1A2A2A05069562 and NRF-2021R1A2C2008235) and by the Basic Science Research Program through the National Research Foundation of Korea (NRF) funded by the Ministry of Science, ICT and Future Planning (NRF-R1A4A1031574) (E.-T.H.), and by an MRC Career Development Award (MR/M021157/1 R.W.M) jointly funded by the U.K. Medical Research Council and Department for International Development and a Wellcome Trust Discovery Award (225844/Z/22/Z) (R.W.M.).

T.-K.N. contributed to the conceptual framework, data curation, formal analysis, investigation, methodology, validation, visualization, and writing the original draft; S.-T.N. and V.-T.N. assisted with data curation and validation; J.S., Y.L.L., S.T.-N., and F.L. supported for data curation and provided resources; S.-H.N., S.-K.L., and R.W.M. contributed resources, validation, and participated in review and editing; W.-S.P. and W.-J.C. were involved in review and editing; J.-H.H. contributed to conceptualization, validation, and review and editing; E.-T.H. led conceptualization, funding acquisition, project administration, resources, supervision, validation, and contributed to writing the original draft, review and editing. All authors had access to the data, and the final decision to submit was made collectively by the authors. The authors declare that the research was conducted in the absence of any commercial or financial relationships that could be construed as a potential conflict of interest.

AUTHOR AFFILIATIONS

¹Department of Medical Environmental Biology and Tropical Medicine, Kangwon National University School of Medicine, Chuncheon-si, Gangwon-do, South Korea

²Institute of Clinical Infectious Diseases, 108 Military Central Hospital, Hanoi, Vietnam

³Department of Obstetrics and Gynecology, Kangwon National University School of Medicine, Chuncheon-si, Gangwon-do, South Korea

⁴Department of Infection Biology, Faculty of Infectious and Tropical Diseases, London School of Hygiene and Tropical Medicine, London, England, United Kingdom

⁵Mahidol Vivax Research Unit, Faculty of Tropical Medicine, Mahidol University, Bangkok, Thailand

⁶Department of Parasitology, Faculty of Medicine, Universiti Malaya, Kuala Lumpur, Malaysia

⁷Department of Physiology, School of Medicine, Kangwon National University, Chuncheon-si, Gangwon-do, South Korea

⁸Department of Pharmacology, School of Medicine, Kangwon National University, Chuncheon-si, Gangwon-do, South Korea

⁹Department of Pathogen Biology and Immunology, School of Medicine, Yangzhou University, Yangzhou, Jiangsu, China

AUTHOR ORCIDs

Robert W. Moon  <http://orcid.org/0000-0002-9070-4292>

Jin-Hee Han  <https://orcid.org/0000-0003-0836-6675>

Eun-Taek Han  <http://orcid.org/0000-0003-1962-7199>

FUNDING

Funder	Grant(s)	Author(s)
National Research Foundation of Korea	NRF-2017R1A2A2A05069562, NRF-2021R1A2C2008235, NRF-R1A4A1031574	Eun-Taek Han
U.K. Medical Research Council and Department for International Development and a Wellcome Trust Discovery Awards	MR/M021157/1, 225844/Z/22/Z	Robert W. Moon

AUTHOR CONTRIBUTIONS

Tuyet-Kha Nguyen, Conceptualization, Data curation, Formal analysis, Investigation, Methodology, Validation, Visualization, Writing – original draft | Sy-Thau Nguyen, Data curation, Validation | Van-Truong Nguyen, Data curation, Validation | Sung-Hun Na, Resources, Writing – review and editing | Robert W. Moon, Resources, Validation, Writing – review and editing | Jetsumon Sattabongkot, Data curation, Resources | Yee Ling Lau, Data curation, Resources | Won-Sun Park, Writing – review and editing | Wan-Joo Chun, Writing – review and editing | Feng Lu, Data curation, Resources | Seong-Kyun Lee, Validation, Writing – review and editing | Jin-Hee Han, Conceptualization, Validation, Writing – review and editing | Eun-Taek Han, Conceptualization, Funding acquisition, Project administration, Resources, Supervision, Validation, Writing – original draft, Writing – review and editing

ETHICS APPROVAL

All relevant guidelines and regulations were followed, and all experimental protocols involving human samples were approved by the Kangwon National University Hospital Ethical Committee (IRB No. KNUH-B-2021-06-034 and 2016-04-005), Medical Research Ethics Committee (MREC), Ministry of Health, Malaysia (National Medical Research

Register ID No. 13079), and Faculty of Tropical Medicine, Mahidol University in Thailand. Written informed consent was obtained from all subjects. The animal study was reviewed and approved by the Institutional Animal Care and Use Committee of Kangwon National University, and the experiments were conducted according to the Ethical Guidelines for Animal Experiments of Kangwon National University (KW-220620-3).

ADDITIONAL FILES

The following material is available [online](#).

Supplemental Material

Supplemental figures (mBio03917-24-s0001.pdf). Fig. S1 to S5.

Supplemental tables (mBio03917-24-s0002.pdf). Tables S1 to S9.

REFERENCES

- Bledsoe GH. 2005. Malaria primer for clinicians in the United States. *South Med J* 98:1197–1204. <https://doi.org/10.1097/01.smj.0000189904.50838.eb>
- Greenwood BM, Targett GAT. 2011. Malaria vaccines and the new malaria agenda. *Clin Microbiol Infect* 17:1600–1607. <https://doi.org/10.1111/j.1469-0691.2011.03612.x>
- De SL, Ntumngia FB, Nicholas J, Adams JH. 2021. Progress towards the development of a *P. vivax* vaccine. *Expert Rev Vaccines* 20:97–112. <https://doi.org/10.1080/14760584.2021.1880898>
- Hou MM, Barrett JR, Themistocleous Y, Rawlinson TA, Diouf A, Martinez FJ, Nielsen CM, Lias AM, King LDW, Edwards NJ, et al. 2023. Vaccination with *Plasmodium vivax* Duffy-binding protein inhibits parasite growth during controlled human malaria infection. *Sci Transl Med* 15:eadf1782. <https://doi.org/10.1126/scitranslmed.adf1782>
- Chen E, Salinas ND, Ntumngia FB, Adams JH, Tolia NH. 2015. Structural analysis of the synthetic Duffy Binding Protein (DBP) antigen DEKnull relevant for *Plasmodium vivax* malaria vaccine design. *PLoS Negl Trop Dis* 9:e0003644. <https://doi.org/10.1371/journal.pntd.0003644>
- VanBuskirk KM, Cole-Tobian JL, Baisor M, Sevova ES, Bockarie M, King CL, Adams JH. 2004. Antigenic drift in the ligand domain of *Plasmodium vivax* duffy binding protein confers resistance to inhibitory antibodies. *J Infect Dis* 190:1556–1562. <https://doi.org/10.1086/424852>
- Kocken CH, Dubbel MA, Van Der Wel A, Pronk JT, Waters AP, Langermans JA, Thomas AW. 1999. High-level expression of *Plasmodium vivax* apical membrane antigen 1 (AMA-1) in *Pichia pastoris*: strong immunogenicity in Macaca mulatta immunized with *P. vivax* AMA-1 and adjuvant SBAS2. *Infect Immun* 67:43–49. <https://doi.org/10.1128/IAI.67.1.43-49.1999>
- Kanjee U, Rangel GW, Clark MA, Duraisingh MT. 2018. Molecular and cellular interactions defining the tropism of *Plasmodium vivax* for reticulocytes. *Curr Opin Microbiol* 46:109–115. <https://doi.org/10.1016/j.mib.2018.10.002>
- Thera MA, Doumbo OK, Coulibaly D, Laurens MB, Ouattara A, Kone AK, Guindo AB, Traore K, Traore I, Kouriba B, et al. 2011. A field trial to assess A blood-stage malaria vaccine. *N Engl J Med* 365:1004–1013. <https://doi.org/10.1056/NEJMoa1008115>
- Ogutu BR, Apollo OJ, McKinney D, Okoth W, Siangla J, Dubovsky F, Tucker K, Waitumbi JN, Diggs C, Wittes J, et al. 2009. Blood stage malaria vaccine eliciting high antigen-specific antibody concentrations confers no protection to young children in Western Kenya. *PLoS One* 4:e4708. <https://doi.org/10.1371/journal.pone.0004708>
- von Itzstein M, Plebanski M, Cooke BM, Coppel RL. 2008. Hot, sweet and sticky: the glycobiology of *Plasmodium falciparum*. *Trends Parasitol* 24:210–218. <https://doi.org/10.1016/j.pt.2008.02.007>
- Muh F, Kim N, Nyunt MH, Firdaus ER, Han J-H, Hoque MR, Lee S-K, Park J-H, Moon RW, Lau YL, Kaneko O, Han E-T. 2020. Cross-species reactivity of antibodies against *Plasmodium vivax* blood-stage antigens to *Plasmodium knowlesi*. *PLoS Negl Trop Dis* 14:e0008323. <https://doi.org/10.1371/journal.pntd.0008323>
- Ndegwa DN, Kundu P, Hostetler JB, Marin-Menendez A, Sanderson T, Mwikali K, Verzier LH, Coyle R, Adjalley S, Rayner JC. 2021. Using *Plasmodium knowlesi* as a model for screening *Plasmodium vivax* blood-stage malaria vaccine targets reveals new candidates. *PLoS Pathog* 17:e1008864. <https://doi.org/10.1371/journal.ppat.1008864>
- Singh B, Daneshvar C. 2013. Human infections and detection of *Plasmodium knowlesi*. *Clin Microbiol Rev* 26:165–184. <https://doi.org/10.1128/CMR.00079-12>
- Mohring F, Hart MN, Rawlinson TA, Henrici R, Charleston JA, Diez Benavente E, Patel A, Hall J, Almond N, Campino S, Clark TG, Sutherland CJ, Baker DA, Draper SJ, Moon RW. 2019. Rapid and iterative genome editing in the malaria parasite *Plasmodium knowlesi* provides new tools for *P. vivax* research. *Elife* 8:e45829. <https://doi.org/10.7554/eLife.45829>
- Crosnier C, Wanaguru M, McDade B, Osier FH, Marsh K, Rayner JC, Wright GJ. 2013. A library of functional recombinant cell-surface and secreted *P. falciparum* merozoite proteins. *Mol Cell Proteomics* 12:3976–3986. <https://doi.org/10.1074/mcp.O113.028357>
- Hostetler JB, Sharma S, Bartholdson SJ, Wright GJ, Fairhurst RM, Rayner JC. 2015. A library of *Plasmodium vivax* recombinant merozoite proteins reveals new vaccine candidates and protein-protein interactions. *PLoS Negl Trop Dis* 9:e0004264. <https://doi.org/10.1371/journal.pntd.0004264>
- Li J, Ito D, Chen J-H, Lu F, Cheng Y, Wang B, Ha K-S, Cao J, Torii M, Sattabongkot J, Tsuboi T, Han E-T. 2012. Pv12, a 6-Cys antigen of *Plasmodium vivax*, is localized to the merozoite rhoptry. *Parasitol Int* 61:443–449. <https://doi.org/10.1016/j.parint.2012.02.008>
- Cheng Y, Lu F, Tsuboi T, Han E-T. 2013. Characterization of a novel merozoite surface protein of *Plasmodium vivax*, Pv41. *Acta Trop* 126:222–228. <https://doi.org/10.1016/j.actatropica.2013.03.002>
- Miller LH, Mason SJ, Dvorak JA, McGinniss MH, Rothman IK. 1975. Erythrocyte receptors for (*Plasmodium knowlesi*) malaria: Duffy blood group determinants. *Science* 189:561–563. <https://doi.org/10.1126/science.1145213>
- Montemiglio LC, Testi C, Ceci P, Falvo E, Pitea M, Savino C, Arcovito A, Peruzzi G, Baiocco P, Mancia F, Boffi A, des Georges A, Vallone B. 2019. Cryo-EM structure of the human ferritin-transferrin receptor 1 complex. *Nat Commun* 10:1121. <https://doi.org/10.1038/s41467-019-09098-w>
- Malleret B, El Sahili A, Tay MZ, Carissimo G, Ong ASM, Novera W, Lin J, Suwanarusk R, Kosaisavee V, Chu TTT, et al. 2021. *Plasmodium vivax* binds host CD98hc (SLC3A2) to enter immature red blood cells. *Nat Microbiol* 6:991–999. <https://doi.org/10.1038/s41564-021-00939-3>
- Lee S-K, Crosnier C, Valenzuela-Leon PC, Dizon BLP, Atkinson JP, Mu J, Wright GJ, Calvo E, Gunalan K, Miller LH. 2024. Complement receptor 1 is the human erythrocyte receptor for *Plasmodium vivax* erythrocyte binding protein. *Proc Natl Acad Sci U S A* 121:e2316304121. <https://doi.org/10.1073/pnas.2316304121>
- Cheng Y, Wang Y, Ito D, Kong D-H, Ha K-S, Chen J-H, Lu F, Li J, Wang B, Takashima E, Sattabongkot J, Tsuboi T, Han E-T. 2013. The *Plasmodium vivax* merozoite surface protein 1 paralogue is a novel erythrocyte-binding ligand of *P. vivax*. *Infect Immun* 81:1585–1595. <https://doi.org/10.1128/IAI.01117-12>
- Lu F, Li J, Wang B, Cheng Y, Kong D-H, Cui L, Ha K-S, Sattabongkot J, Tsuboi T, Han E-T. 2014. Profiling the humoral immune responses to *Plasmodium vivax* infection and identification of candidate immunogenic rhoptry-associated membrane antigen (RAMA). *J Proteomics* 102:66–82. <https://doi.org/10.1016/j.jprot.2014.02.029>
- Sy Thau N, Nguyen T-K, Truong NV, Chu T-T, Na S-H, Moon RW, Lau YL, Nyunt MH, Park W-S, Chun W-J, Lu F, Lee S-K, Han J-H, Han E-T. 2024. Characterization of merozoite-specific thrombospondin-related anonymous protein (MTRAP) in *Plasmodium vivax* and *P. knowlesi*

- parasites. *Front Cell Infect Microbiol* 14:1354880. <https://doi.org/10.3389/fcimb.2024.1354880>
27. Cheng Y, Lu F, Wang B, Li J, Han J-H, Ito D, Kong D-H, Jiang L, Wu J, Ha K-S, Takashima E, Sattabongkot J, Cao J, Nyunt MH, Kyaw MP, Desai SA, Miller LH, Tsuboi T, Han E-T. 2016. *Plasmodium vivax* GPI-anchored micronemal antigen (PvGAMA) binds human erythrocytes independent of Duffy antigen status. *Sci Rep* 6:35581. <https://doi.org/10.1038/srep35581>
 28. Han J-H, Lee S-K, Wang B, Muh F, Nyunt MH, Na S, Ha K-S, Hong S-H, Park WS, Sattabongkot J, Tsuboi T, Han E-T. 2016. Identification of a reticulocyte-specific binding domain of *Plasmodium vivax* reticulocyte-binding protein 1 that is homologous to the PFRh4 erythrocyte-binding domain. *Sci Rep* 6:26993. <https://doi.org/10.1038/srep26993>
 29. Cheng Y, Wang B, Changrob S, Han J-H, Sattabongkot J, Ha K-S, Chootong P, Lu F, Cao J, Nyunt MH, Park WS, Hong S-H, Lim CS, Tsuboi T, Han E-T. 2017. Naturally acquired humoral and cellular immune responses to *Plasmodium vivax* merozoite surface protein 8 in patients with *P. vivax* infection. *Malar J* 16:1–12. <https://doi.org/10.1186/s12936-017-1837-5>
 30. Wang B, Lu F, Han J-H, Lee S-K, Cheng Y, Nyunt MH, Ha K-S, Hong S-H, Park WS, Han E-T. 2016. Characterization of caveola-vesicle complexes (CVCs) protein, PHIST/CVC-8195 in *Plasmodium vivax*. *Korean J Parasitol* 54:725–732. <https://doi.org/10.3347/kjp.2016.54.6.725>
 31. Muh F, Lee S-K, Hoque MR, Han J-H, Park J-H, Firdaus ER, Moon RW, Lau YL, Han E-T. 2018. In vitro invasion inhibition assay using antibodies against *Plasmodium knowlesi* Duffy binding protein alpha and apical membrane antigen protein 1 in human erythrocyte-adapted *P. knowlesi* A1-H.1 strain. *Malar J* 17:1–11. <https://doi.org/10.1186/s12936-018-2420-4>
 32. Muh F, Ahmed MA, Han J-H, Nyunt MH, Lee S-K, Lau YL, Kaneko O, Han E-T. 2018. Cross-species analysis of apical asparagine-rich protein of *Plasmodium vivax* and *Plasmodium knowlesi*. *Sci Rep* 8:5781. <https://doi.org/10.1038/s41598-018-23728-1>
 33. Longley RJ, Grigg MJ, Schoffer K, Obadia T, Hyslop S, Piera KA, Nekkab N, Mazhari R, Takashima E, Tsuboi T, Harbers M, Tetteh K, Drakeley C, Chitnis CE, Healer J, Tham W-H, Sattabongkot J, White MT, Cooper DJ, Rajahram GS, Barber BE, William T, Anstey NM, Mueller I. 2022. *Plasmodium vivax* malaria serological exposure markers: assessing the degree and implications of cross-reactivity with *P. knowlesi*. *Cell Rep Med* 3:100662. <https://doi.org/10.1016/j.xcrm.2022.100662>
 34. Verzier LH, Coyle R, Singh S, Sanderson T, Rayner JC. 2019. *Plasmodium knowlesi* as a model system for characterising *Plasmodium vivax* drug resistance candidate genes. *PLoS Negl Trop Dis* 13:e0007470. <https://doi.org/10.1371/journal.pntd.0007470>
 35. Taechalertpaisarn T, Crosnier C, Bartholdson SJ, Hodder AN, Thompson J, Bustamante LY, Wilson DW, Sanders PR, Wright GJ, Rayner JC, Cowman AF, Gilson PR, Crabb BS. 2012. Biochemical and functional analysis of two *Plasmodium falciparum* blood-stage 6-cys proteins: P12 and P41. *PLoS One* 7:e41937. <https://doi.org/10.1371/journal.pone.0041937>
 36. Kar S, Sinha A. 2022. *Plasmodium vivax* Duffy binding protein-based vaccine: a distant dream. *Front Cell Infect Microbiol* 12:916702. <https://doi.org/10.3389/fcimb.2022.916702>
 37. Devi YS, Mukherjee P, Yazdani SS, Shakri AR, Mazumdar S, Pandey S, Chitnis CE, Chauhan VS. 2007. Immunogenicity of *Plasmodium vivax* combination subunit vaccine formulated with human compatible adjuvants in mice. *Vaccine (Auckl)* 25:5166–5174. <https://doi.org/10.1016/j.vaccine.2007.04.080>
 38. Durocher Y, Perret S, Kamen A. 2002. High-level and high-throughput recombinant protein production by transient transfection of suspension-growing human 293-EBNA1 cells. *Nucleic Acids Res* 30:e9. <https://doi.org/10.1093/nar/30.2.e9>
 39. Tom R, Bisson L, Durocher Y. 2008. Transfection of HEK293-EBNA1 cells in suspension with linear PEI for production of recombinant proteins. *Cold Spring Harb Protoc* 2008:2008.pdb.prot4977. <https://doi.org/10.1101/pdb.prot4977>
 40. Nguyen TS, Park J-H, Nguyen T-K, Nguyen TV, Lee S-K, Na S-H, Han J-H, Park W-S, Chun W, Lu F, Han E-T. 2023. *Plasmodium vivax* merozoite-specific thrombospondin-related anonymous protein (PvMTRAP) interacts with human CD36, suggesting a novel ligand-receptor interaction for reticulocyte invasion. *Parasit Vectors* 16:426. <https://doi.org/10.1186/s13071-023-06031-5>
 41. Wittig I, Braun H-P, Schägger H. 2006. Blue native PAGE. *Nat Protoc* 1:418–428. <https://doi.org/10.1038/nprot.2006.62>
 42. Chen J-H, Jung J-W, Wang Y, Ha K-S, Lu F, Lim CS, Takeo S, Tsuboi T, Han E-T. 2010. Immunoproteomics profiling of blood stage *Plasmodium vivax* infection by high-throughput screening assays. *J Proteome Res* 9:6479–6489. <https://doi.org/10.1021/pr100705g>
 43. Moon RW, Hall J, Rangkuti F, Ho YS, Almond N, Mitchell GH, Pain A, Holder AA, Blackman MJ. 2013. Adaptation of the genetically tractable malaria pathogen *Plasmodium knowlesi* to continuous culture in human erythrocytes. *Proc Natl Acad Sci U S A* 110:531–536. <https://doi.org/10.1073/pnas.1216457110>
 44. Moon RW, Sharaf H, Hastings CH, Ho YS, Nair MB, Rchiad Z, Knuepfer E, Ramaprasad A, Mohring F, Amir A, Yusuf NA, Hall J, Almond N, Lau YL, Pain A, Blackman MJ, Holder AA. 2016. Normocyte-binding protein required for human erythrocyte invasion by the zoonotic malaria parasite *Plasmodium knowlesi*. *Proc Natl Acad Sci U S A* 113:7231–7236. <https://doi.org/10.1073/pnas.1522469113>
 45. Hart MN, Mohring F, DonVito SM, Thomas JA, Muller-Siennerth N, Wright GJ, Knuepfer E, Saibil HR, Moon RW. 2023. Sequential roles for red blood cell binding proteins enable phased commitment to invasion for malaria parasites. *Nat Commun* 14:4619. <https://doi.org/10.1038/s41467-023-40357-z>
 46. Mohring F, Hart MN, Patel A, Baker DA, Moon RW. 2020. CRISPR-Cas9 genome editing of *Plasmodium knowlesi*. *Bio Protoc* 10:e3522. <https://doi.org/10.21769/BioProtoc.3522>
 47. Bae S, Kweon J, Kim HS, Kim JS. 2014. Microhomology-based choice of Cas9 nuclease target sites. *Nat Methods* 11:705–706. <https://doi.org/10.1038/nmeth.3015>
 48. Ribaut C, Berry A, Chevalley S, Reybier K, Morlais I, Parzy D, Nepveu F, Benoit-Vical F, Valentin A. 2008. Concentration and purification by magnetic separation of the erythrocytic stages of all human *Plasmodium* species. *Malar J* 7:45. <https://doi.org/10.1186/1475-2875-7-45>